Journal of Crystal Growth 329 (2011) 57–61

Contents lists available at ScienceDirect

Journal of Crystal Growth

journal homepage: www.elsevier.com/locate/jcrysgro

Investigating the chemical and morphological evolution of GaAs capped InAs/InP quantum dots emitting at 1.5 μm using aberration-corrected scanning transmission electron microscopy

S. Kadkhodazadeh [a,b,*], E.S. Semenova [b], K. Yvind [b], R.E. Dunin-Borkowski [a,c]

[a] Center for Electron Nanoscopy, Technical University of Denmark, DK 2800 Lyngby, Denmark
[b] Department of Photonics Engineering, Technical University of Denmark, DK 2800 Lyngby, Denmark
[c] Ernst Ruska Center (ER-C) and Peter Grünberg Institute (PGI), Research Center Jülich, 52425 Jülich, Germany

ARTICLE INFO

Article history:
Received 8 February 2011
Received in revised form
23 May 2011
Accepted 20 June 2011
Communicated by M.S. Goorsky
Available online 30 June 2011

Keywords:
A1. Characterisation
A1. Nanostructures
A1. Scanning transmission electron microscopy
A3. Metalorganic vapour-phase epitaxy
A3. Quantum dots
B2. Semiconducting III/V materials

ABSTRACT

The emission wavelength of InAs quantum dots grown on InP has been shown to shift to the technologically desirable 1.5 μm with the deposition of 1–2 monolayers of GaAs on top of the quantum dots. Here, we use aberration-corrected scanning transmission electron microscopy to investigate morphological and compositional changes occurring to the quantum dots as a result of the deposition of 1.7 monolayers of GaAs on top of them, prior to complete overgrowth with InP. The results are compared with theoretical models describing the overgrowth process.

1. Introduction

Self-assembled semiconductor quantum dots (QDs) are of interest for a wide range of applications that include optical amplifiers, temperature-stable low noise lasers and mode-locked lasers (e.g. [1–3]). For applications in optical communication great effort has been devoted for tuning the emission wavelength of InAs QDs to the fibre-optics-compatible 1.5 μm (e.g. [4,5]). As the structural properties of the QDs, such as their morphology and chemical composition, largely determine their optical properties, a detailed understanding of these parameters is needed to control the growth process. To date, the majority of the characterisation work carried out on InAs QDs has been on InAs/GaAs structures (e.g. [6–8]). However, despite the successful application of InAs/GaAs QD structures emitting at 1.3 μm (e.g.[9]). the extension of the emission wavelength of these structures remains challenging. More recently, the growth of InAs/InP QDs by metalorganic vapour-phase epitaxy (MOVPE) has been developed and shown to be promising for 1.5 μm emission wavelength applications (e.g. [10–13]). The smaller lattice mismatch between InAs and InP, compared to that between InAs and GaAs, results in the formation of larger QDs on InP than on GaAs, for the same amount of InAs deposited. InAs/InP QDs typically emit at wavelengths above 1.7 μm. Several techniques such as double capping growth [12] or the insertion of a GaAs underlayer [13] have been used to control the size of the QDs and tune their emission wavelength to the desired 1.5 μm range. For example, inserting a thin layer of GaAs or GaP below the QDs in InAs/InGaAsP QD structures was shown to tune the room-temperature emission wavelength of the QDs within the range 1.5–1.6 μm [13].

Here, we describe the results of an aberration-corrected scanning transmission electron microscopy (STEM) study of the structural properties of InAs QDs grown on InP, for which partial capping with 1.7 monolayers (ML) of GaAs prior to capping with InP was found to decrease the room-temperature emission wavelength to the desired 1.5 μm (the results of our optical characterisation will be discussed in a future publication). We use atomic-resolution STEM to identify changes introduced to the QDs by partial capping with GaAs. High-angle annular dark-field (HAADF) imaging in STEM can provide an image contrast that is less sensitive to strain [14]. This gives an advantage over

* Corresponding author at: Technical University of Denmark, Centre for Electron Nanoscopy, Fysikvej Building 307, room 115, 2800 Lyngby, Denmark.
E-mail address: shka@fotonik.dtu.dk (S. Kadkhodazadeh).

0022-0248/$ - see front matter © 2011 Elsevier B.V. All rights reserved.
doi:10.1016/j.jcrysgro.2011.06.037

conventional TEM imaging techniques, in which image interpretation is often complicated by the strong strain contrast present. Furthermore, STEM holds the required resolution to characterise the small amounts of the deposited GaAs successfully, which is otherwise challenging using other characterisation techniques.

2. Experimental details

Two samples, A and B, were grown in a vertical low-pressure MOVPE TurboDisc® reactor on InP (0 0 1) substrates, using H_2 as a carrier gas, trimethylindium (TMIn) and trimethilgallium (TMGa) as group III sources and arsine, phosphine and tertiarybutylphosphine (TBP) as group V sources. A RealTemp® system was used for the temperature control during the growth. The following growth sequence was employed: an InP buffer layer was deposited on top of an InP substrate at 610 °C. The temperature was then ramped down to 516 °C under a PH_3 pressure and switched to AsH_3 after the temperature stabilised. Arrays of QDs were formed by the deposition of 1.65ML of InAs onto the InP buffer layer at 516 °C, with a V/III ratio of 4.7 and a growth rate of 1.45 Å/s. Sample A was overgrown with 10 nm of InP after 12 s growth interruption and at low temperature, followed by a further 5 nm of InP at 610 °C. The QDs in sample B were initially overgrown with 1.7ML of GaAs, followed by further overgrowth with InP as for Sample A.

Cross-sectional and plan-view specimens were prepared by mechanical polishing and dimpling, followed by argon ion milling. They were examined at 300 kV using an FEI Titan instrument that is fitted with a field-emission electron source and a spherical aberration corrector on the condenser lens system. The electron probe convergence semi-angle used was 17.5 mrad, the electron probe diameter was 1.5 Å and the HAADF inner and outer detector semi-angles were 60 and 300 mrad, respectively. The specimen thickness was calculated using the log-ratio model in electron energy-loss spectroscopy, as described in [15].

3. Results and discussion

Fig. 1 shows cross-sectional high-resolution HAADF STEM images of samples A and B aligned along the [$\bar{1}$ 1 0] zone-axis. Under the experimental conditions employed here, the image contrast is sensitive primarily to variations in the atomic number (Z-contrast imaging). The QDs appear as bright regions, primarily due to the higher atomic number of As compared to *P*. The QDs in Sample A are on average 22.6 ± 2.0 nm in width and 3.1 ± 0.2 nm (10.5 ± 0.8ML) in height (measured from 10 different dots) while the dots in sample B are on average 23.5 ± 1.8 nm in width and 2.0 ± 0.2 nm (7.0 ± 0.8ML) in height (measured from 14 different dots). These observations suggest that the deposition of 1.7ML of GaAs onto the QDs in sample B has resulted in an average reduction of 3.5ML in the heights of the QDs.

In addition to the difference in image intensity between regions of different chemical composition, a difference is visible between the shapes of the atomic-resolution contrast features in the P-rich and As-rich regions. When InAs or GaAs crystals are viewed along ⟨1 1 0⟩ type zone-axis specimen orientations, the contrast from both the neighbouring In/Ga and As columns is visible, resulting in atomic contrast that is commonly referred to as a dumbbell structure [16]. However, in the case of InP, only the contrast from In atomic columns is visible as the contrast from the columns of P atoms is much weaker, and hence, the dumbbell contrast features are no longer visible. Corresponding simulated STEM images of InP, InAs and GaAs produced using the multislice simulation software QSTEM [17], for three different specimen thicknesses and using the same instrumental parameters as those used in the experiments, are shown in Fig. 2(d), (e) and (f), respectively. The same difference between the shapes of the atomic-scale contrast features for InAs or GaAs and InP is observed in the simulated images.

A region containing the edge of a QD in sample B and the wetting layer next to it is shown in Fig. 2(a). The marked area in Fig. 2(a) is enlarged in Fig. 2(b) to better display the shapes of the diatomic columns. The thickness of the wetting layer seen in HAADF STEM images of the QDs in Sample A was found to be ~2ML. However, in sample B, a further 3ML of dumbbell-shaped diatomic columns can be seen above the wetting layer (see Fig. 2(b)) but was not seen in similar regions in Sample A. This means that a further 3ML of As-rich material is present above the wetting layer in sample B. This pattern was observed everywhere on the wetting layer around the QDs in sample B (position 1 in Fig. 2(c)), but was not observed close to the tops of the QDs (position 2 in Fig. 2(c)). This dumbbell-like contrast can be sensitive to the number of As atoms relative to P atoms from the surrounding InP matrix, along the viewed direction. In the case of a uniform distribution of the capping GaAs over the QDs in sample B, up to 2ML of dumbbell-like contrast is expected to be present above the wetting layer, as well as above the QDs. The intensity of the dumbbell-like contrast is then expected to decrease towards the tops of the QDs, since the ratio of As to P atoms present in this orientation decreases towards the tops of the QDs. Fig. 2(g) shows a simulated image of the atomic-resolution contrast expected to be seen above the tops of the QDs (position 2 in Fig. 2(c)) in a 50 nm thick specimen, in the case of a uniform distribution of GaAs. The QDs have flat tops of approximately 15 nm. Therefore, the simulation was carried out for 15 nm of GaAs encapsulated in the middle of 35 nm of InP. Although the dumbbell-like contrast is not as pronounced as that seen in pure InAs or GaAs (Fig. 2(e) and (f), respectively), it can

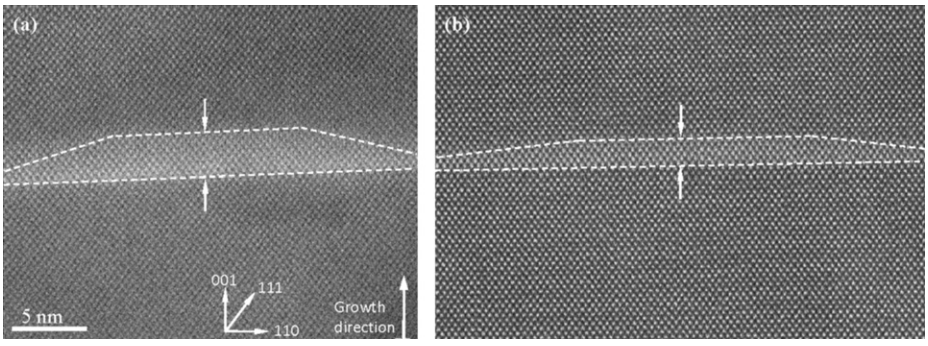

Fig. 1. High-resolution Z-contrast HAADF STEM images of (a) Sample A and (b) sample B in cross-sectional geometry. The dotted lines mark the outline of the QDs and the arrows denote the measured height of them. Both specimens are oriented along the [$\bar{1}$ 1 0] zone-axis.

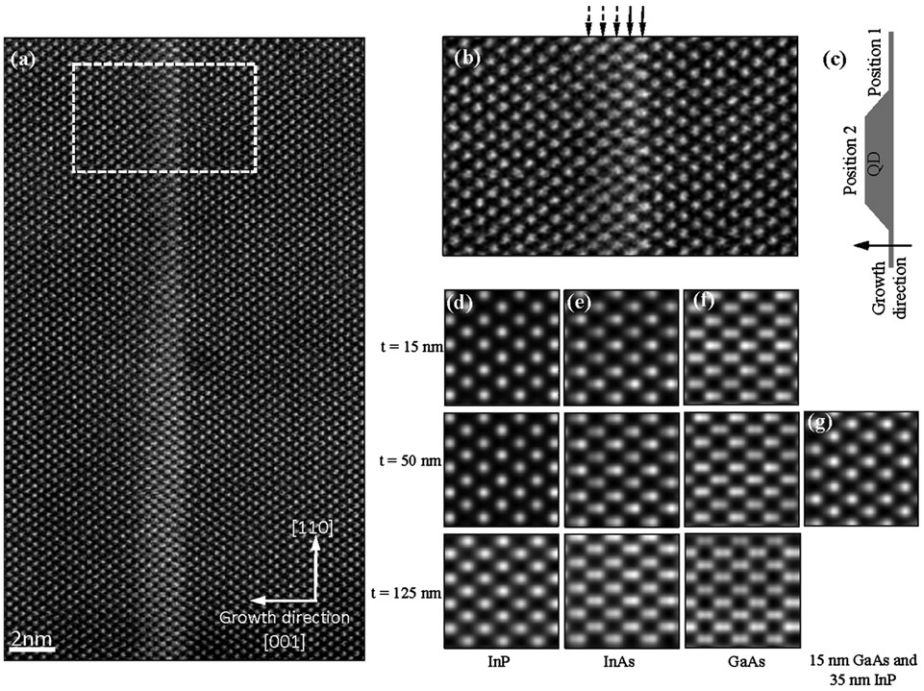

Fig. 2. (a) Cross-sectional HAADF STEM image of part of QD and the wetting layer in sample B acquired along the [$\bar{1}$ 1 0] zone-axis. (b) The marked region in (a) zoomed in and the contrast and brightness in the image is enhanced. The solid arrows denote the 2ML of wetting layer and the dotted arrows denote the 3ML of As-rich region above it. (c) A schematic showing two different positions relative to the QDs discussed in the text. (d), (e) and (f) Simulated HAADF STEM images of InP, InAs and GaAs, respectively, along ⟨1 1 0⟩ type zone-axis for specimen thicknesses, t=15, 50 and 125 nm. The field of view in each image is approximately 18nm × 18 nm. (g) Simulated HAADF STEM image of a 50 nm thick specimen containing 15 nm of GaAs encapsulated in the middle of 35 nm of InP, along a ⟨1 1 0⟩ type zone-axis. Simulations were carried out using the QSTEM software and using the same instrumental parameters as those used in the experiments, including electron beam accelerating voltage of 300 kV, electron probe convergence semi-angle of 17.5 mrad and probe diameter of 1.5 Å [17].

still be recognised in the simulated image in Fig. 2(g). However, no dumbbell-like features above the tops of the QDs are visible in the experimental images. This combined with the presence of 3ML of this contrast feature over the wetting layer, around the bases of the QDs (position 1 in Fig. 2(c)) suggests that GaAs may have segregated around the QDs in this sample.

In order to better understand the influence of the deposited GaAs on the morphology of the QDs in sample B, energy-dispersive X-ray spectroscopy (EDS) of the QDs was carried out in both cross-sectional and plan-view specimen geometries. Consistently, lower levels of Ga were measured on the tops of the QDs, while higher levels of Ga were detected around the QDs. Examples of the EDS analyses are shown in Fig. 3. The measured ratios between the Ga and In signals detected at each point marked in Fig. 3(a) and (c) are shown in Fig. 3(b) and (d), respectively. The inset in Fig. 3(a) shows the expected beam broadening in EDS, which results in the collection of a signal from regions that are approximately 1–2 nm in size at each acquisition point [18]. The higher level of Ga detected at point 2 in Fig. 3(a), when compared with points 1 and 3, may result from the presence of Ga above and below the QD in the electron beam direction. This explanation is supported by the plan-view analysis shown in Figs. 3(c) and (d), where the strongest Ga signal is detected around the QDs (*e.g.* points 1, 4 and 6), while minimal amounts of Ga are detected at the position of the QDs (*e.g.* points 3 and 5).

The high-resolution HAADF STEM images and EDS analysis suggest that the deposition of 1.7ML of GaAs leads to a reduction in the heights of the QDs and to the presence of GaAs primarily around the bases of the QDs. These morphological changes then lead to the reduction of the emission wavelength of the QDs to the desired value of 1.5 μm. Our observations are consistent with theoretical models of the overgrowth processes of QDs, in which the initial stage of overgrowth is said to be driven by strain relaxation and leads to a height reduction of the QDs [19–21]. Prior to overgrowth, the tops of the QDs are the least strained positions within the QDs, where the lattice parameter approaches that of bulk InAs [22]. However, overgrowing the QDs with a material of smaller lattice parameter makes the tops of the QDs the least favourable positions for the adsorption of the overgrowth material. Instead, the overgrowth material is suggested to cause InAs to migrate away from the tops of the QDs and redistribute around the bases of the QDs. A larger lattice mismatch between the dot material and the capping material is expected to cause higher degrees of structural modifications during overgrowth. This behaviour explains the greater height reduction of the QDs in sample B as compared to Sample A, due to the larger lattice mismatch between InAs and GaAs (7% mismatch) as compared to that between InAs and InP (3% mismatch). This process leads to the segregation of an alloy of the capping material and InAs around the bases of the dots. The 3ML of As-rich material observed on top of the wetting layer in high-resolution HAADF STEM images of the QDs in sample B (Fig. 2) is therefore likely to be InGaAs, formed by alloying between the capping GaAs and the InAs that was removed from the tops of the dots.

4. Conclusions

We have used aberration-corrected STEM and EDS to investigate morphological changes in InAs QDs grown on InP(0 0 1) resulting from partial overgrowth of the dots by 1.7ML of GaAs. HAADF STEM imaging and EDS analysis suggest that the observed

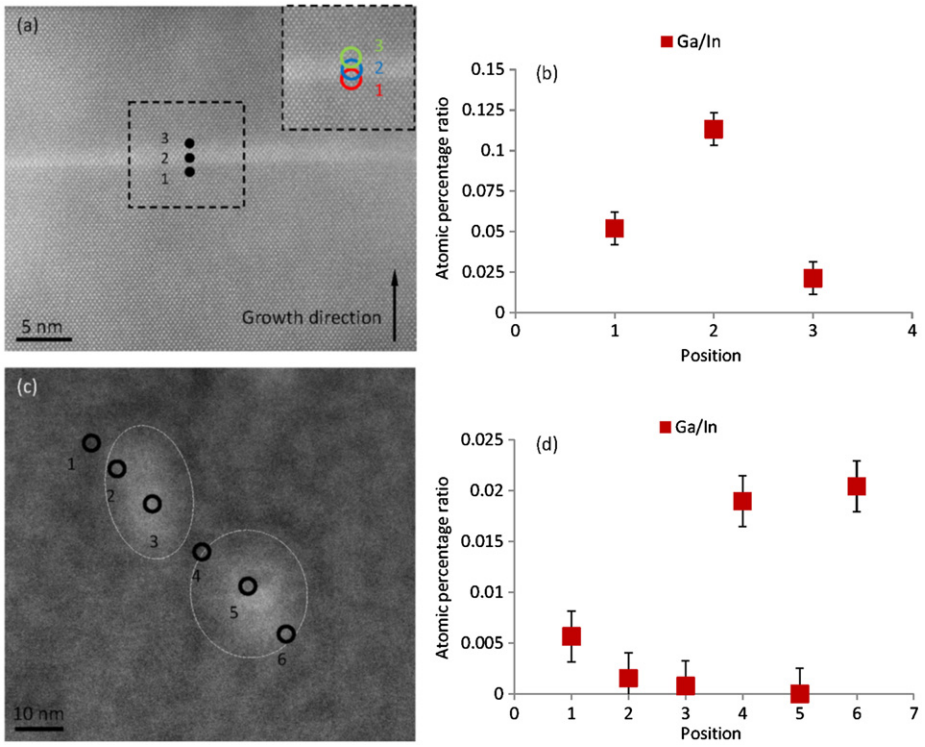

Fig. 3. (a) Cross-sectional and (c) plan-view HAADF STEM images of QDs in sample B. The outlines of the QDs in (c) are marked with dotted lines. (b) and (d) The ratios of the Ga/In signals detected by EDS at each acquisition point marked in images (a) and (c). The specimen thickness is estimated to be ~50 nm in (a) and ~30 nm in (c). The acquisition time was 60 s at each point. The plan-view specimen in (c) was only ion-milled from the back and there is 15 nm of InP above the QDs. The inset in image (a) shows the extent of the estimated broadening effect in EDS.

reduction in the average heights of the QDs following overgrowth is associated with redistribution of the deposited GaAs around the bases of the QDs. Our results are consistent with the theoretical models describing overgrowth processes of QDs. Such changes in the morphologies of the QDs lead to a change in their emission wavelength to 1.5 μm, which is desired for optical communication applications.

Acknowledgements

This work was financially supported by the Danish Technical Research Council through the research programme Optical Sampling for Coherent Detection Receivers (OPSCODER) and QUantum dot structures Enabling light Slow-down and amplificaTion (QUEST) and through the Villum Kann Rasmussen Centre of excellence NATEC. The A P Møller and Chastine Mc-Kinney Møller Foundation are gratefully acknowledged for their contribution towards the establishment of the Centre for Electron Nanoscopy in the Technical University of Denmark. E.S. Semenova thanks the European Commission for funding through a Marie Curie Incoming International Fellowship (project number 252890). The authors would like to thank Martin Schubert for fruitful discussions.

References

[1] T. Akiyama, Y. Arakawa, Quantum dot semiconductor optical amplifier, Proc. IEEE 95 (2007) 1757–1766.
[2] M. Sugawara, M. Usami, Quantum dot devices: handling the heat, Nat. Photonics 3 (2009) 30–31.
[3] M.G. Thompson, A.R. Rae, M. Xia, R.V. Penty, I.H. White, InGaAs Quantum-dot mode-locked laser diodes, IEEE J. Sel. Top. Quantum Electron. 15 (2009) 661–672.
[4] H. Saito, K. Nishi, S. Sugou, Ground-state lasing at room temperature in long-wavelength InAs quantum dot lasers on InP(311)B substrate, Appl. Phys. Lett 78 (2001) 267–269.
[5] R. Schwertberger, D. Gold, J.P. Reithmaier, A. Forchel, Epitaxial growth of 1.55 μm emitting InAs quantum dashes on InP-based heterostructures by GS-MBE for long-wavelength laser applications, J. Cryst. Growth 251 (2003) 248–252.
[6] P. Wang, A.L. Bleloch, M. Faluk, P.J. Goodhew, J. Ng, M. Missous, Direct measurement of composition of buried quantum dots using aberration-corrected scanning transmission electron microscopy, Appl. Phys. Lett. 89 (2006) 72111.
[7] G. Costantini, A. Rastelli, C. Manzano, R. Songmuang, O.G. Schmidt, K. Kern, H. von Kanel, Universal shapes of self-organised semiconductor quantum dots: striking similarities between InAs/GaAs(0 0 1) and Ge/Si(0 0 1), Appl. Phys. Lett. 85 (2004) 5673–5675.
[8] T. Inoue, T. Kita, O. Wada, M. Konno, T. Yaguchi, T. Kamino, Electron tomography of embedded semiconductor quantum dots,, Appl. Phys. Lett. 92 (2008) 031902.
[9] T.J. Badcock, R.J. Royce, D.J. Mowbray, M.S. Skolnick, H.Y. Liu, M. Hopkinson, K.M. Groom, Q. Jiang, Low-threshold current density and negative characteristic temperature 1.3 μm InAs self-assembled quantum dot lasers, Appl. Phys. Lett. 90 (2007) 111102.
[10] A. Anantathanasarn, R. Nötzel, P.J. van Veldhoven, F.W.M. van Otten, T.J. Eijkemans, Y. Barbarin, T. de Vries, E. Smalbrugge, E.J. Geluk, E.A.J.M. Bente, Y.S. Oei, M.K. Smit, J.H. Wolter, Stacking, polarization control, and lasing of wavelength tunable (1.55 mm region) InAs/InGaAsP/InP(1 0 0) quantum dots, J. Cryst. Growth 298 (2007) 553–557.
[11] A. Michon, G. Saint-Girons, G. Beaudoin, I. Sagnes, L. Largeau, G. Patriarche, InAs/InP(0 0 1) quantum dots emitting at 1.55 μm grown by low-pressure metal-organic vapour epitaxy, Appl. Phys. Lett. 87 (2005) 253114.
[12] Z.G. Lu, J.R. Liu, P.J. Poole, S. Raymond, P.J. Barrios, D. Poitras, G. Pakulski, P. Grant, D. Roy-Guay, An L-band monolithic InAs/InP quantum dot mode-locked laser with femtosecond pulses, Opt. Express 17 (2009) 13609–13614.
[13] Q. Gong, R. Nötzel, P.J. van Veldhoven, J.H. Wolter, InAs/InP quantum dots emitting in the 1.55 mm wavelength region by inserting ultrathin GaAs and GaP interlayers, J. Cryst. Growth 278 (2005) 67–71.
[14] D.E. Jesson, S.J. Pennycook, Incoherent imaging of thin specimens using coherently scattered electrons, Proc. R. Soc. London A 441 (1993) 261–281.

[15] R.F. Egerton, Electron Energy-loss Spectroscopy in the Electron Microscope, second ed., Plenum Press, New York, 1996, pp. 302–307.
[16] J. Liu, J.M. Cowley, High-resolution scanning transmission electron microscopy, Ultramicroscopy 52 (1993) 335–346.
[17] C.T. Koch, Determination of Core Structure Periodicity and Point Defect Density along Dislocations, Ph.D. Thesis, ()Arizona State University, 2002.
[18] J.M. Titchmarsh, Comparison of high spatial resolution in EDX and EELS analysis, Ultramicroscopy 28 (1989) 347–351.
[19] C. Costantini, A. Rastelli, C. Manzano, P. Acosta-Diaz, R. Songmuang, G. Katsaros, O.G. Schmidt, K. Kern, Interplay between thermodynamics and kinetics in the capping of InAs/GaAs(0 0 1) quantum dots, Phys. Rev. Lett. 96 (2006) 226106.
[20] X.L. Li, G.W. Yang, Thermodynamic theory of shape evolution induced by Si capping in Ge quantum dot self-assembly, J. Appl. Phys. 105 (2009) 13510.
[21] P.B. Joyce, T.J. Krzyzewski, G.R. Bell, T.S. Jones, Surface morphology evolution during the overgrowth of large InAs–GaAs quantum dots, Appl. Phys. Lett. 79 (2001) 3615.
[22] V.G. Stoleru, D. Pal, E. Towe, Self-assembled (In,Ga)As /GaAs quantum-dot nanostructures: strain distribution and electronic structure, Phys E: Low Dimension Systems Nanostruct 15 (2002) 131.